The Influences of the Gyro Sensors' Errors on the Attitude Calculus

Teodor Lucian Grigorie [1], Dragos George Sandu [2]
[1] University of Craiova, Faculty of Electrical Engineering, 107 Decebal Blvd., Craiova, Dolj, Romania
[2] Flight Test Center, 1 Gl. Stefan Ispas Str., Craiova, Dolj, Romania
E-mail: *lgrigore@elth.ucv.ro*

Abstract – *The paper presents a study about the weight of the different errors of the gyro sensors in the error of attitude angles calculus. For study three types of gyros are selected in order to emphasize the differences in performance currently existing between these categories and the way in which these performances are reflected on to the errors of the attitude angles. To evaluate the errors, the gyros are modeled in Matlab/Simulink using the information from the data sheets and a Savage method to integrate the attitude equation is used. We will further emphasize the influences of noise, bias, gyros accuracy to measure different accelerations and scale factor's calibration error.*

Keywords – *Inertial Navigation, Strap-Down Systems, Gyrometric sensors, Sensors errors, Attitude angles*

1. INTRODUCTION

According to the cinematic equations of speed and position, very well-known in classical mechanics, the vehicle's current speed equals the initial speed plus the time integral of the cinematic acceleration while the current position equals the initial position plus the time integral of the speed. On board the vehicle, the final value of the acceleration is calculated by adding the gravitational acceleration with the acceleration produced by the non-gravitational forces applied on the vehicle. To determine the acceleration modulus and sense we generally use accelerometers but the acceleration is a vector also characterized by a direction. The way of determining the direction of the total acceleration led to the appearance of the two fundamental systems for the inertial navigation: the stabilized platform INS and strap-down INS [1].

For the first one, we use a set of gyros to maintain the accelerometers oriented in a known direction as reported to a fixed, non-rotating frame which is linked to the inertial space. The gyros and accelerometers are put on a gyroscopically suspended platform with the gyros controlling the suspensions loops. For this instance, the calculus for the speed and position are highly simplified, as the attitude angles are given first-hand by the gyros on the platform. So, the requests for precision are low as these gyros are concerned [2].

For the second case, the accelerometers and gyros are rigidly put on the vehicle's structure so they move together with the vehicle frame. This condition results in the name of the system: INS strap-down, or as a literary translation, INS with fix components. Thus, the gyros measure the aircraft's absolute rotation speed and give the accelerometers' instantaneous orientation in order to deduce the speed and position [2].

The position errors result from the partial knowledge of the initial conditions, from the inertial system's numerical calculus and from gyros and accelerometers errors. So, the inertial sensors' accuracy has a main role in the evaluation of navigation system's precision, a system which comprises all of them, and as a result, they must be considered when designing one.

The following material presents an evaluation of the influence of parameters and errors from three gyros on the attitude angles got from the solving of the Poisson attitude quaternionic equation with a Savage algorithm. The evaluation starts from the Matlab/Simulink model of the three gyros on the bases of the data from their data sheets. We will further emphasize the influences of noise, bias, gyros accuracy to measure different accelerations and scale factor's calibration error.

2. GYROS MODELATION

The optoelectronic gyros apparition and their superior performances as compared to the mechanical gyros led to their large usage in strap-down inertial navigation systems. Thus, in the '90 years IEEE specialists started to use standardization of testing procedures for the main types of such gyros (laser gyros [3] and interferometric fiber optic gyros [4]). Present tendencies related to the miniaturization of inertial navigation systems had on the rotation sensors a similar impact to the acceleration sensors. Thus, MEMS technology strongly developed to this direction. As a result miniaturized gyros were produced. Their functioning principle is mainly based on the presence of Coriolis forces induced by the rotation movement which was to be detected. An IEEE recent standard stipulates the testing procedures to be used for the vibrations Coriolis gyros [5].

In the specialized literature the vast majority of

numerical simulations from strap-down inertial navigation systems suppose the presence of clean acceleration and rotation signals on the input, without noises and errors. The study on the errors of navigation systems is generally done without considering the sensors' errors.

In order to put up a complex study as accurate as possible from the point of view of real conditions for the navigation system and which to include the real errors of the used sensors, we can produce an equivalent model to the IEEE one. It has to consider the parameters from the data sheets offered by the sensors producers and to allow the making of studies, as accurate as possible, for the strap-down inertial navigation systems. Such a model is described in the formula

$$\omega = (\omega_i + S \cdot a_r + B + \nu)(1 + \Delta K / K), \qquad (1)$$

where ω is the output angular speed (disturbed signal), ω_i is the input angular speed, S is sensitivity to the acceleration a_r applied upon an arbitrary direction, B the bias, K the scale factor, ΔK the calibration error of the scale factor and ν the sensor's noise. The physical data involved in the model described in formula (1) are measured as: angular speeds ω and ω_i in $^\circ/\mathrm{s}$, sensitivity S in $(^\circ/\mathrm{s})/\mathrm{g}$, acceleration a_r in g, B in percents from the length of the measurement interval (span), K in $\mathrm{mV}/(^\circ/\mathrm{s})$, ΔK in percents from K and the noise ν is given by its density ν_d measured in $(^\circ/\mathrm{s})/\sqrt{\mathrm{Hz}}$.

Based on the model described in equation (1) it results a Matlab/Simulink model good for gyros in general, which considers the parameters variation limits as offered by the producers in the data sheets (Fig. 1). The model reflects the fact that the bias is given as a maximum value B as a percentage from span, the scale factor calibration error is given as its absolute maximum value ΔK as a percentage from K, and the noise is given by the maximum value of its density.

The block resulted from the grouping of the schema in Fig. 1 a. Is presented in Fig. 1 b., having as inputs the angular velocity ω_i applied along the sensor's sensibility axes and the acceleration a_r considered to be the resulting acceleration system (the resultant of the accelerations applied on the 3 directions on the accelerometric triad from the strap-down inertial system), non-disturbed, and as output disturbed angular speed ω.

The model contains the predefined parameters for three gyro sensors, electronic and opto-electronic, made in MEMS technology or in a classical way. The change in the gyro sensor to be used in simulations is made with the help of the interface in Fig. 2. The interface also allows the setting of the model by the user in a custom variant, with the manual introducing of parameters in the specific fields. The model can be used in the numerical simulation of the strap-down inertial navigation systems in very close to reality conditions from the point of view of the distortions suffered by the signal of angular speed when passing through any type of gyro implemented in the navigator.

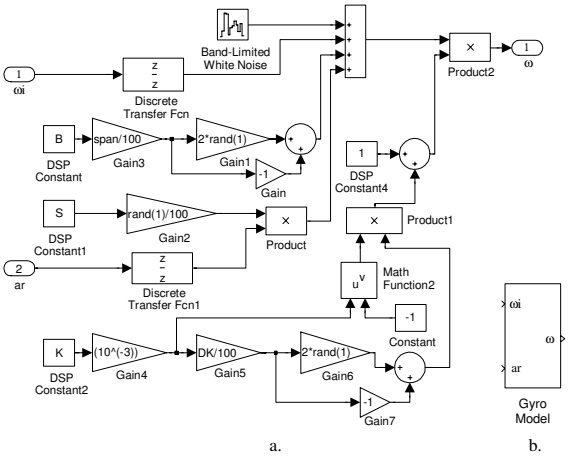

Fig. 1. Matlab/Simulink gyros model

For study we selected 3 types of gyros in order to emphasize the differences in performance currently existing between these categories and the way in which these performances are reflected on to the errors of the attitude angles. The first gyro is a MEMS whose functioning is based on the Coriolis forces, the second one is a fiber optic gyro (FOG) while the third one is a laser gyro.

From Table 1 we can notice that the laser gyro sensor, frequently used in inertial navigators, has superior performances as compared to the gyro realized in MEMS technology. The fiber optic gyro sensor, however, show close performances being a serious competitor due to low fabrication costs and to the conception „solid state" put up in integrated optics technology which also gives a certain degree of miniaturization.

Table 1. The parameters of gyro sensors

Sensor type	Gyro MEMS	FOG	Gyro Laser
Measurement range [^{o}/s]	±500	±150	±1000
Scale factor [mV/(^{o}/s)]	10	65	20
Bandwidth [Hz]	60	100	500
Noise density [(^{o}/s)/$\sqrt{\mathrm{Hz}}$]	0,0035	0,0084	$5{,}8 \cdot 10^{-6}$
Bias [% of span]	0,1	$1{,}7 \cdot 10^{-4}$	$9{,}8 \cdot 10^{-8}$
Scale factor error [%]	1	0,02	$5{,}2 \cdot 10^{-4}$
Sensitivity to accelerations [(^{o}/s)/g]	0,02	0	0

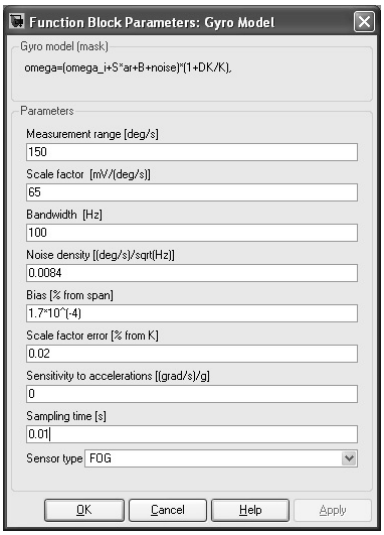

Fig. 2. Parameters setting for the gyros error model

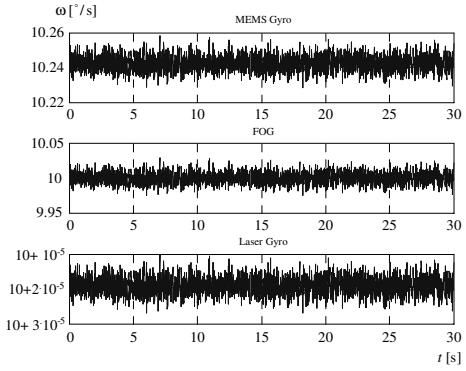

Fig. 3. Model's output for the gyros at inputs $\omega_i = 10\ ^{o}/\text{s}$ and $a_r = 10\ \text{m/s}^2 \cong 1\,g$

By applying an input angular speed $\omega_i = 10\ ^{o}/\text{s}$ to this created model, in the presence of the acceleration signal $a_r = 10\ \text{m/s}^2 \cong 1\,g$ we get the disturbed signals from Fig. 3. Thus, analyzing the amplitudes touched by noise we conclude that the laser gyro and fiber optic gyro are less noisy than MEMS gyro. There is also to be mentioned the powerful influence of the other errors, especially the bias and the miss calibration error of the scale factor, on the signal applied at MEMS sensor input.

3. ATTITUDE ANGLES CALCULUS

In a quaternionic form, the Poisson equation is

$$\dot{Q} = \frac{\mathrm{d}Q}{\mathrm{d}t} = \frac{1}{2}\vec{\underline{\omega}} \cdot Q, \tag{2}$$

when Q is the quaternion which realize the transformation between the mobile frame m and the inertial frame I, and $\vec{\underline{\omega}}$ is the quaternion associated to the absolute angular speed vector $\vec{\omega}$ of the mobile frame m,

$$\vec{\underline{\omega}} = \omega_x \cdot i + \omega_y \cdot j + \omega_z \cdot k. \tag{3}$$

If we denote by q_0, q_1, q_2, q_3 the components of the quaternion Q, with the formula (3), equation (2) becomes

$$\begin{bmatrix} \dot{q}_1 \\ \dot{q}_2 \\ \dot{q}_3 \\ \dot{q}_0 \end{bmatrix} = \frac{1}{2}\begin{bmatrix} 0 & \omega_z & -\omega_y & \omega_x \\ -\omega_z & 0 & \omega_x & \omega_y \\ \omega_y & -\omega_x & 0 & \omega_z \\ -\omega_x & -\omega_y & -\omega_z & 0 \end{bmatrix} \cdot \begin{bmatrix} q_1 \\ q_2 \\ q_3 \\ q_0 \end{bmatrix}. \tag{4}$$

In addition of the Poisson equation numerical integration, we take care that to each actualization of the matrix R_m^I it must be orthonormalized,

$$R_m^I \cdot \left(R_m^I\right)^T = \left(R_m^I\right)^T \cdot R_m^I = I_3, \tag{5}$$

and the components of the new quaternion satisfy the relation

$$q_0^2 + q_1^2 + q_2^2 + q_3^2 = 1. \tag{6}$$

So, the integration algorithms must be followed by the orthonormalization algorithms for matrix, or for the quaternion.

According with Savage [6], the new quaternion can be calculated with the formula

$$(Q)_{\mathrm{n}} = Q(t_n) = Q(t_{n-1}) \cdot Q_{m(t_n)}^{m(t_{n-1})} = (Q)_{\mathrm{o}} \cdot Q_{m(t_n)}^{m(t_{n-1})}, \tag{7}$$

where $Q_{m(t_n)}^{m(t_{n-1})}$ is the quaternion which characterize the orientation of the mobile frame m at the t_{n-1} time relative to its orientation at the t_n time. The formal definition of the quaternion $Q_{m(t_n)}^{m(t_{n-1})}$ is [6]

$$Q_{m(t_n)}^{m(t_{n-1})} = \underline{1} + \int_{t_{n-1}}^{t_n} \dot{Q}_{m(t)}^{m(t_{n-1})}\,\mathrm{d}t, \tag{8}$$

when $m(t)$ describes the attitude of the frame m at the arbitrary time t, into the interval $t_{n-1} \div t_n$, and $\underline{1}$ is the unity quaternion.

Also, the quaternion $Q_{m(t_n)}^{m(t_{n-1})}$ can be expressed in terms of a rotation vector ϕ_n which defines the attitude of the frame $m(t_n)$ relative to the $m(t_{n-1})$ frame [6]

$$Q_{m(t_n)}^{m(t_{n-1})} = \cos\frac{|\phi_n|}{2} + \frac{1}{|\phi_n|}\sin\frac{|\phi_n|}{2}(\phi_x i + \phi_y j + \phi_z k), \tag{9}$$

with ϕ_x, ϕ_y and ϕ_z - the components of the ϕ_n vector. In matriceal form we have [6]

$$\begin{bmatrix} q_1 \\ q_2 \\ q_3 \\ q_0 \end{bmatrix}_{\mathrm{n}} = \left[\cos\frac{|\phi_n|}{2} \cdot I_4 + \frac{2}{|\phi_n|} \sin\frac{|\phi_n|}{2} \cdot \hat{\phi}_n \right] \begin{bmatrix} q_1 \\ q_2 \\ q_3 \\ q_0 \end{bmatrix}_{\mathrm{o}}, \quad (10)$$

with

$$\begin{aligned} \phi_x(t_n) &= \alpha_x(t_n) + \beta_x(t_n), \\ \phi_y(t_n) &= \alpha_y(t_n) + \beta_y(t_n), \\ \phi_z(t_n) &= \alpha_z(t_n) + \beta_z(t_n). \end{aligned} \quad (11)$$

Considering l calculus steps in the time interval $t_{n-1} \div t_n$, we obtain the relations

$$\Delta\alpha_x(t_l) = \int_{t_{l-1}}^{t_l} \omega_x \mathrm{d}t, \ \Delta\alpha_y(t_l) = \int_{t_{l-1}}^{t_l} \omega_y \mathrm{d}t, \ \Delta\alpha_z(t_l) = \int_{t_{l-1}}^{t_l} \omega_z \mathrm{d}t, \quad (12)$$

$$\begin{aligned} \alpha_x(t_l) &= \alpha_x(t_{l-1}) + \Delta\alpha_x(t_l), \\ \alpha_y(t_l) &= \alpha_y(t_{l-1}) + \Delta\alpha_y(t_l), \\ \alpha_z(t_l) &= \alpha_z(t_{l-1}) + \Delta\alpha_z(t_l), \end{aligned} \quad (13)$$

in initial conditions

$$\alpha_x(t_l) = \alpha_y(t_l) = \alpha_z(t_l) = 0 \text{ at } t_l = t_{n-1}. \quad (14)$$

It results

$$\begin{aligned} \alpha_x(t_n) &= \alpha_x(t_l), \\ \alpha_y(t_n) &= \alpha_y(t_l), \\ \alpha_z(t_n) &= \alpha_z(t_l) \text{ at } t_l = t_n, \end{aligned} \quad (15)$$

$$\begin{aligned} \Delta\beta_x(t_l) &= \frac{1}{2}\left[\alpha_y(t_{l-1}) + \frac{1}{6}\Delta\alpha_y(t_{l-1})\right]\alpha_z(t_l) - \\ &\quad - \frac{1}{2}\left[\alpha_z(t_{l-1}) + \frac{1}{6}\Delta\alpha_z(t_{l-1})\right]\alpha_y(t_l), \\ \Delta\beta_y(t_l) &= \frac{1}{2}\left[\alpha_z(t_{l-1}) + \frac{1}{6}\Delta\alpha_z(t_{l-1})\right]\alpha_x(t_l) - \\ &\quad - \frac{1}{2}\left[\alpha_x(t_{l-1}) + \frac{1}{6}\Delta\alpha_x(t_{l-1})\right]\alpha_z(t_l), \\ \Delta\beta_z(t_l) &= \frac{1}{2}\left[\alpha_x(t_{l-1}) + \frac{1}{6}\Delta\alpha_x(t_{l-1})\right]\alpha_y(t_l) - \\ &\quad - \frac{1}{2}\left[\alpha_y(t_{l-1}) + \frac{1}{6}\Delta\alpha_y(t_{l-1})\right]\alpha_x(t_l), \end{aligned} \quad (16)$$

$$\begin{aligned} \beta_x(t_l) &= \beta_x(t_{l-1}) + \Delta\beta_x(t_l), \\ \beta_y(t_l) &= \beta_y(t_{l-1}) + \Delta\beta_y(t_l), \\ \beta_z(t_l) &= \beta_z(t_{l-1}) + \Delta\beta_z(t_l), \end{aligned} \quad (17)$$

in initial conditions

$$\beta_x(t_l) = \beta_y(t_l) = \beta_z(t_l) = 0 \text{ at } t_l = t_{n-1}. \quad (18)$$

So, we obtain

$$\begin{aligned} \beta_x(t_n) &= \beta_x(t_l), \\ \beta_y(t_n) &= \beta_y(t_l), \\ \beta_z(t_n) &= \beta_z(t_l) \text{ at } t_l = t_n, \end{aligned} \quad (19)$$

from the equations (12)÷(19), it results the vector ϕ_n components (11), and the norm

$$|\phi_n| = \sqrt{\phi_x^2(t_n) + \phi_y^2(t_n) + \phi_z^2(t_n)}. \quad (20)$$

Taking into account the matrix

$$\hat{\phi}_n = \frac{1}{2}\begin{bmatrix} 0 & \phi_z(t_n) & -\phi_y(t_n) & \phi_x(t_n) \\ -\phi_z(t_n) & 0 & \phi_x(t_n) & \phi_y(t_n) \\ \phi_y(t_n) & -\phi_x(t_n) & 0 & \phi_z(t_n) \\ -\phi_x(t_n) & -\phi_y(t_n) & -\phi_z(t_n) & 0 \end{bmatrix} \quad (21)$$

and Taylor developments of the coefficients of the matrices I_4 and $\hat{\phi}_n$, from the relation (10) it results

$$\begin{aligned} \cos\frac{|\phi_n|}{2} &= 1 - \frac{1}{2!}\left(\frac{|\phi_n|}{2}\right)^2 + \frac{1}{4!}\left(\frac{|\phi_n|}{2}\right)^4 - \ldots, \\ \frac{2}{|\phi_n|}\cos\frac{|\phi_n|}{2} &= 1 - \frac{1}{3!}\left(\frac{|\phi_n|}{2}\right)^2 + \frac{1}{5!}\left(\frac{|\phi_n|}{2}\right)^4 - \ldots, \end{aligned} \quad (22)$$

which, through truncation, gives the actualization formula for the rotation quaternion

$$\begin{aligned} \begin{bmatrix} q_1 \\ q_2 \\ q_3 \\ q_0 \end{bmatrix}_{\mathrm{n}} &= \left\{ \left[1 - \frac{1}{2!}\left(\frac{|\phi_n|}{2}\right)^2 + \frac{1}{4!}\left(\frac{|\phi_n|}{2}\right)^4 - \ldots \right] \cdot I_4 + \right. \\ &\quad \left. + \left[1 - \frac{1}{3!}\left(\frac{|\phi_n|}{2}\right)^2 + \frac{1}{5!}\left(\frac{|\phi_n|}{2}\right)^4 - \ldots \right] \cdot \hat{\phi}_n \right\} \begin{bmatrix} q_1 \\ q_2 \\ q_3 \\ q_0 \end{bmatrix}_{\mathrm{o}}. \end{aligned} \quad (23)$$

By the quaternion orthonormalization algorithm, we have the norm

$$|Q(t_{n+1})| = \sqrt{q_0^2(t_{n+1}) + q_1^2(t_{n+1}) + q_2^2(t_{n+1}) + q_3^2(t_{n+1})} \quad (24)$$

and the new values of the quaternion's parameters [7], [8], [9]

$$\begin{aligned} q_1(t_{n+1}) &= \frac{q_1(t_{n+1})}{|Q(t_{n+1})|}, \ q_2(t_{n+1}) = \frac{q_2(t_{n+1})}{|Q(t_{n+1})|}, \\ q_3(t_{n+1}) &= \frac{q_3(t_{n+1})}{|Q(t_{n+1})|}, \ q_0(t_{n+1}) = \frac{q_0(t_{n+1})}{|Q(t_{n+1})|}. \end{aligned} \quad (25)$$

Considering the equivalent matrix of the attitude quaternion [7], [8], [9]

$$R_t^v = \begin{bmatrix} q_0^2+q_1^2-q_2^2-q_3^2 & 2(q_1q_2+q_0q_3) & 2(q_1q_3-q_0q_2) \\ 2(q_1q_2-q_0q_3) & q_0^2+q_2^2-q_1^2-q_3^2 & 2(q_2q_3+q_0q_1) \\ 2(q_1q_3+q_0q_2) & 2(q_3q_2-q_0q_1) & q_0^2+q_3^2-q_1^2-q_2^2 \end{bmatrix}, \quad (26)$$

it results

$$\begin{aligned} r_{11}(t_{n+1}) &= q_0^2(t_{n+1})+q_1^2(t_{n+1})-q_2^2(t_{n+1})-q_3^2(t_{n+1}), \\ r_{12}(t_{n+1}) &= 2\left[q_1(t_{n+1})q_2(t_{n+1})+q_0(t_{n+1})q_3(t_{n+1})\right], \\ r_{13}(t_{n+1}) &= 2\left[q_1(t_{n+1})q_3(t_{n+1})-q_0(t_{n+1})q_2(t_{n+1})\right], \\ r_{21}(t_{n+1}) &= 2\left[q_1(t_{n+1})q_2(t_{n+1})-q_0(t_{n+1})q_3(t_{n+1})\right], \\ r_{22}(t_{n+1}) &= q_0^2(t_{n+1})+q_2^2(t_{n+1})-q_1^2(t_{n+1})-q_3^2(t_{n+1}), \\ r_{23}(t_{n+1}) &= 2\left[q_3(t_{n+1})q_2(t_{n+1})+q_0(t_{n+1})q_1(t_{n+1})\right], \\ r_{31}(t_{n+1}) &= 2\left[q_1(t_{n+1})q_3(t_{n+1})+q_0(t_{n+1})q_2(t_{n+1})\right], \\ r_{32}(t_{n+1}) &= 2\left[q_2(t_{n+1})q_3(t_{n+1})-q_0(t_{n+1})q_1(t_{n+1})\right], \\ r_{33}(t_{n+1}) &= q_0^2(t_{n+1})+q_3^2(t_{n+1})-q_1^2(t_{n+1})-q_2^2(t_{n+1}). \end{aligned} \quad (27)$$

But, the direction cosine matrix, which makes the shift between the vehicle frame and local horizontal frame, can be also obtained by three successive rotations, its elements equal [7]

$$\begin{aligned} r_{11} &= \cos\theta\cos\psi, \\ r_{12} &= \cos\theta\sin\psi, \\ r_{13} &= -\sin\theta, \\ r_{21} &= \sin\varphi\sin\theta\cos\psi-\cos\varphi\sin\psi, \\ r_{22} &= \sin\varphi\sin\theta\sin\psi+\cos\varphi\cos\psi, \\ r_{23} &= \sin\varphi\cos\theta, \\ r_{31} &= \cos\varphi\sin\theta\cos\psi+\sin\varphi\sin\psi, \\ r_{32} &= \cos\varphi\sin\theta\sin\psi-\sin\varphi\cos\psi, \\ r_{33} &= \cos\varphi\cos\theta. \end{aligned} \quad (28)$$

Having the values of the matrix elements for the current time moment as well as for the previous one, from the (28) formula we can determine the roll, pitch and yaw angles with the formula

$$\begin{aligned} \varphi &= \mathrm{arctg}(r_{23}/r_{33}), \\ \theta &= \arcsin(-r_{13}), \\ \psi &= \mathrm{arctg}(r_{12}/r_{11}), \end{aligned} \quad (29)$$

where it is important to consider the trigonometric quadrant where the angles are placed.

4. NUMERICAL SIMULATIONS' RESULTS

By implementing the Savage algorithm in an S-function in Matlab („Savage_Attitude"), we get the Matlab/Simulink model of error testing in Fig. 4. To correctly evaluate the errors we apply on input, on the three rotation axes, signals of non-disturbed angular speeds („Signal Builder" blocks). These signals are passed through Savage attitude algorithm in two ways: directly or through a gyro model (that is after they are disturbed by the gyro in the measurement process). The attitude errors due to gyros are calculated as the difference between the attitude angles calculated in these two ways. In order to ease the error calculus and prevent the interference between the three attitude channels, there were applied successive non-null angular speed signals on the three inputs. Because the error level is approximately the same for the three attitude axes, we will further work on the errors from just one channel, the roll.

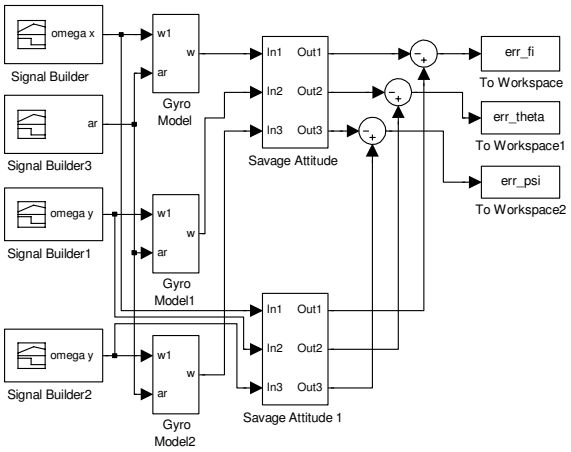

Fig. 4. Matlab/Simulink Simulation Model

At first, we analyze the error values resulted from a null input of angular velocity on the roll axis for 10 s. Simultaneously, at the second input of the „GyroModel" block we apply an acceleration of $a_r = 10\ \mathrm{m/s^2} \cong 1g$. The graphic characteristics are presented in Fig. 5 (Gyro MEMS), Fig. 6 (FOG) and Fig. 7 (Gyro laser). In the figures depicted the roll errors due to bias only ($B \neq 0$), to acceleration sensitivity only ($S \neq 0$), noise only ($\nu \neq 0$), and the ones obtained for all the errors of the gyro sensors. We notice that FOG and Gyro laser have a null sensibility to the linear accelerations, and for Gyro MEMS the dominant error is the bias. This results in a deviation of -2.018 degrees in 10 s for MEMS sensor, -10^{-3} degrees for FOG and $-3.98\cdot10^{-6}$ degree for Gyro laser. The negative values of the deviations due to bias reflect the positive bias values, chosen for the three gyros when performing the simulations. The differences between the errors due to bias equal 3 orders of magnitude in the reports of FOG/MEMS and Gyro laser/FOG. As the noise triggered errors we notice that they are comparable in the cases of Gyro MEMS and FOG and they are 3 orders of magnitude smaller for the Gyro laser. An important percentage from the error induced by the Gyro MEMS is due to the sensor's acceleration sensitivity which produces an error of -0.0168 degrees in 10 s, for an acceleration of approximately 1g. For optical

gyros, the error produced by the bias in 10 s is comparable with the one produced by noise, so, theirs combining may be benefic in some situations.

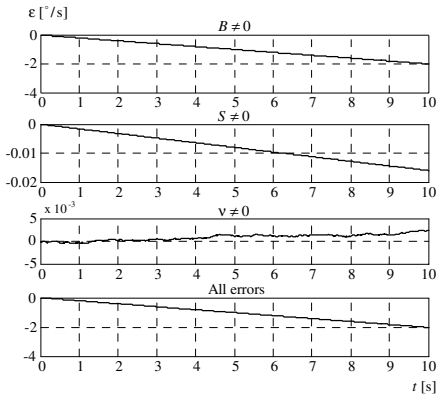

Fig. 5. The answer for Gyro MEMS at $\omega_i = 0\ ^{\circ}/\mathrm{s}$

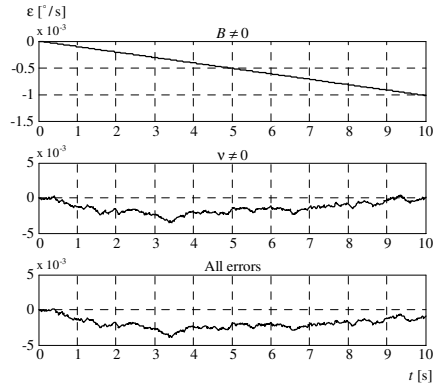

Fig. 6. The answer for FOG at $\omega_i = 0\ ^{\circ}/\mathrm{s}$

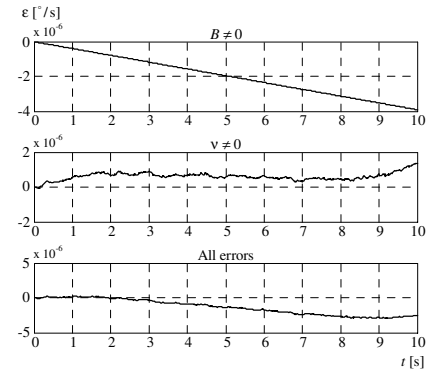

Fig. 7. The answer for Gyro laser at $\omega_i = 0\ ^{\circ}/\mathrm{s}$

To better show the error due to calibration error of the scale factor we apply on input an angular speed $\omega_i = 10\ ^{\circ}/\mathrm{s}$ for 10 s, with the acceleration $a_r = 10\ \mathrm{m/s}^2$. The errors are depicted in Fig. 8 (Gyro MEMS), Fig. 9 (FOG) and Fig. 10 (Gyro laser). We notice that the errors resulted from the wrong calibration of the scale factor equal -0.4 degrees for Gyro MEMS, almost one order of magnitude smaller at FOG (-0.0824 degrees) and three orders of magnitude smaller for Gyro laser ($-2.1 \cdot 10^{-4}$ degrees). At the same time we emphasize the invariant of the other errors with the input data and their increase with the calibration error for the scale factor (to notice the final values of the total error for the two simulated cases).

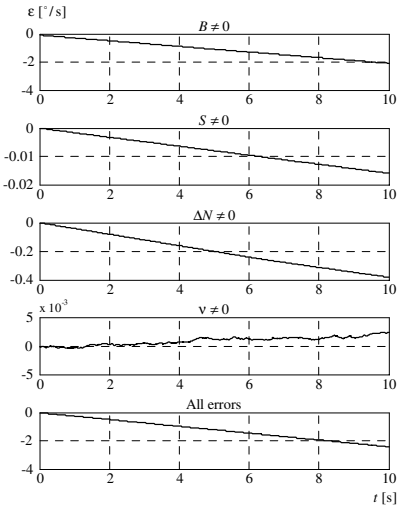

Fig. 8. The answer for Gyro MEMS at $\omega_i = 10\ ^{\circ}/\mathrm{s}$

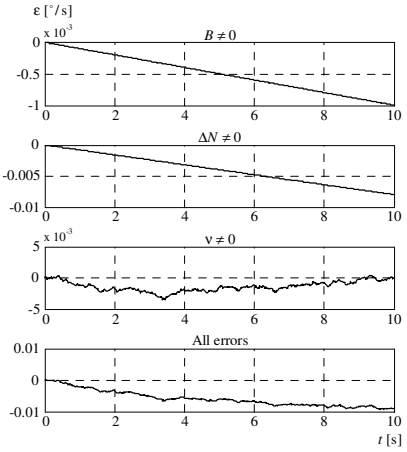

Fig. 9. The answer for FOG at $\omega_i = 10\ ^{\circ}/\mathrm{s}$

By producing numerical simulations for angular speeds applied on input, with values ranging from $-50\ ^{\circ}/\mathrm{s} \div 50\ ^{\circ}/\mathrm{s}$ and $a_r = 10\ \mathrm{m/s}^2 \cong 1g$ for 10 s, we obtain the error surfaces in Fig. 11 (Gyro MEMS), Fig. 12 (FOG) and Fig. 13 (Gyro laser). We notice the error increase with the absolute value of the input angular velocity for all the three cases. The cause is the calibration error of the scale factor. At Gyro MEMS we see an error compensation with the angular velocity getting to $-50\ ^{\circ}/\mathrm{s}$. (due to a large positive value of the bias). Moreover, because of the considered positive values for all the three gyros, we

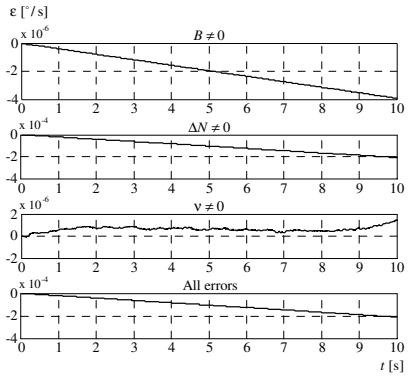

Fig. 10. The answer for Gyro laser at $\omega_i = 10\ ^\circ/\mathrm{s}$

also notice an unbalance between the errors' value for angular speeds of $-50\ ^\circ/\mathrm{s}$, and $50\ ^\circ/\mathrm{s}$. Thus, for Gyro MEMS the error after 10 s is $\varepsilon = -0.2178$ degrees at $\omega_i = -50\ ^\circ/\mathrm{s}$ and $\varepsilon = -4.0216$ degrees at $\omega_i = 50\ ^\circ/\mathrm{s}$. For FOG, after 10 s at $\omega_i = -50\ ^\circ/\mathrm{s}$ the error is positive $\varepsilon = 0.0389$ degrees, and at $\omega_i = 50\ ^\circ/\mathrm{s}$ it is negative, $\varepsilon = -0.0411$ degrees. In a similar way, we get positive error values for Gyro laser, $\varepsilon = 0.001037$ degrees at $\omega_i = -50\ ^\circ/\mathrm{s}$ after 10 s, and negative error values $\varepsilon = -0.001042$ degrees for $\omega_i = 50\ ^\circ/\mathrm{s}$. Practically, the error of the gyros scale factor results in an increase of approximately 1 order of magnitude for the attitude angles' errors due to bias and noise, for an input angular speed of $\omega_i = 50\ ^\circ/\mathrm{s}$ for 10 s. The effect is very visible in FOG and Gyro laser where the errors due to bias and noise are rather low (by orders 10^{-3} and 10^{-6} degrees).

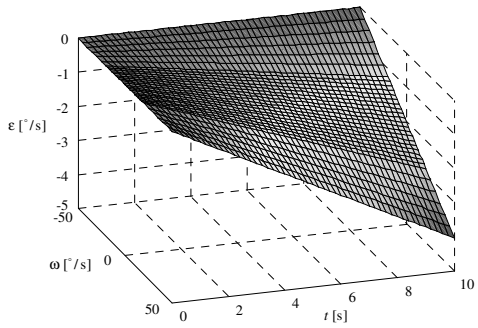

Fig. 11. The answer for Gyro MEMS

To fully demonstrate the evolution of the attitude angles' errors due only to the calibration error of the scale factor, we depicted the error surfaces for angular input speeds, ranging from $-50\ ^\circ/\mathrm{s} \div 50\ ^\circ/\mathrm{s}$; Fig. 14 for Gyro MEMS, Fig. 15 for FOG, and Fig. 16 for Gyro laser. The maximum error values result in the negative value for $\omega_i = 50\ ^\circ/\mathrm{s}$ and in positive value for $\omega_i = -50\ ^\circ/\mathrm{s}$, after 10 s of simulation. Thus, for Gyro MEMS we have $\varepsilon = -2$ degrees and $\varepsilon = 2$ degrees, for FOG $\varepsilon = -0.04$ degrees and $\varepsilon = 0.04$ degrees, and for Gyro laser $\varepsilon = -0.001039$ degrees and $\varepsilon = 0.001039$ degrees.

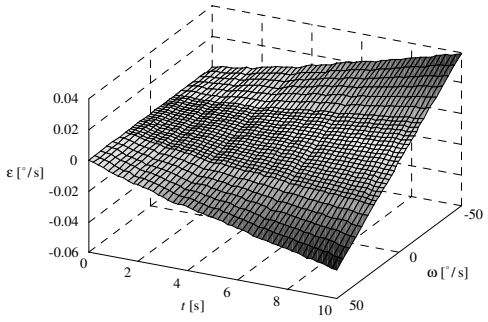

Fig. 12. The answer for FOG

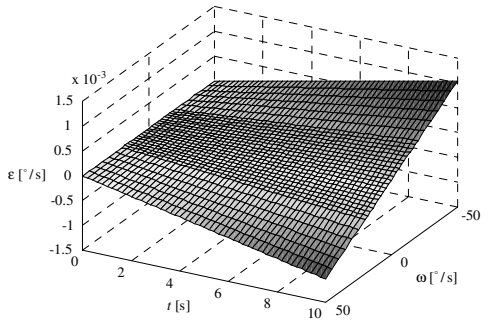

Fig. 13. The answer for Gyro laser

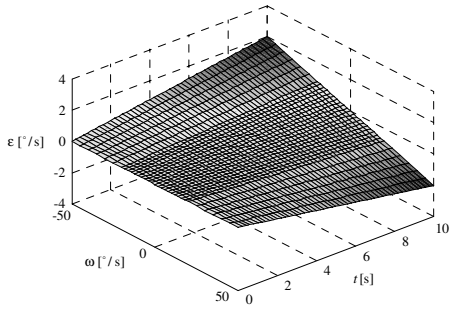

Fig. 14. Error at $\Delta K \neq 0$ for Gyro MEMS

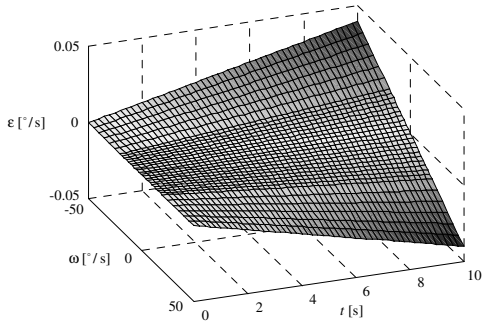

Fig. 15. Error at $\Delta K \neq 0$ for FOG

Considering the dependency of the attitude angles' errors on the Gyro MEMS error due to its

sensibility to linear accelerations we present the error surface in Fig. 17 for acceleration ranging from 0 m/s^2 and 50 m/s^2 and the input angular speed of $\omega_i = 0\ ^\circ/\text{s}$. The maximum value of the attitude error is -0.08 degrees and corresponds to $a_r = 50$ m/s^2.

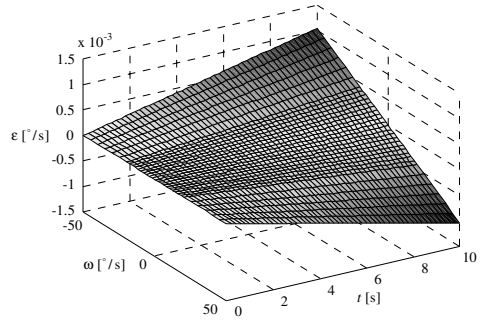

Fig. 16. Error at $\Delta K \neq 0$ for Gyro laser

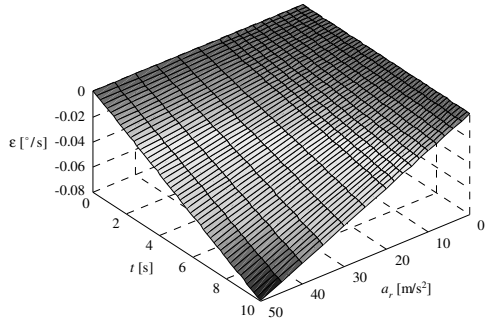

Fig. 17. Error at $S \neq 0$ for Gyro MEMS

5. CONCLUSIONS

The paper is a study of the attitude angles errors produced by the errors of the gyro sensors. This study was made for three sensors categories: Gyro MEMS Coriolis, FOG and Gyro laser. The results emphasize the superior quality of optical sensors as compared to the MEMS. The errors are several orders of magnitude smaller for the first case. Practically, the main sources of errors come from the gyros' bias and their calibration error of the scale factor. Its correction is rather delicate matter, considering that the bias can be corrected, although it can have unpredictable evolutions due to the temperature of the environment. That is why we recommend the usage of optical fiber gyros or gyro laser for the strap-down inertial applications with long duration and high dynamics. For the applications that require a lower precision and are performed at low speed we can use MEMS which previously underwent a bias correction.

REFERENCES

[1] C. Broxmeyer, *Inertial navigation Systems*, McGraw-Hill, New York, 1964

[2] A.B. Chatfield, *Fundamentals of High Accuracy Inertial Navigation*, American Institute of Aeronautics and Astronautics, 1997

[3] IEEE Std. 952-1997, *IEEE Standard Specification Format Guide and Test Procedure for Single-Axis Interferometric Fiber Optic Gyros*, Published by IEEE, New York, USA, September 16, 1997

[4] IEEE Std. 647-1995, *IEEE Standard Specification Format Guide and Test Procedure for Single-Axis Laser Gyros*, Published by IEEE, New York, USA, September 21, 1995

[5] IEEE Std. 1431-2004, *IEEE Standard Specification Format Guide and Test Procedure for Coriolis Vibratory Gyros*, Published by IEEE, New York, USA, *December* 20, 2004

[6] P.G. Savage, „Strapdown Inertial Navigation Integration Algorithm Design Part 1: Attitude Algorithms", *Journal of Guidance, Control, and Dynamics*, Vol. 21, No. 1, Jan.-Feb., 1998

[7] O.S. Salychev, *Inertial Systems in Navigation and Geophysics*, Bauman MSTU Press, Moscow, 1998

[8] J. Farrell, M. Barth, *The Global Positioning System and Inertial Navigation*. McGraw-Hill, New York, 1999

[9] J.C. Radix, *Systèmes inertiels a composants lies <<Strap-Down>>*, Cepadues-Editions, Ecole Nationale Supérieure de l'Aéronautique et de l'Espace SUP'AERO, Toulouse, 1993